

Slip rate at the north-eastern front of the Qilian Shan, China

Jean-Daniel Champagnac,¹ Dao-Yang Yuan,² Wei-Peng Ge,^{2,3} Peter Molnar⁴ and Wen-Jun Zheng³

¹Swiss Federal Institute of Technology, CH-8092 Zurich, Switzerland; ²Lanzhou Institute of Seismology, China Earthquake Administration, Lanzhou 730000, China; ³State Key Laboratory of Earthquake Dynamics, Institute of Geology, China Earthquake Administration, Beijing 100029, China; ⁴Department of Geological Sciences, and Cooperative Institute for Research in Environmental Sciences, University of Colorado, Boulder, CO 80309, USA

ABSTRACT

We constrain the slip rate for the frontal thrust of the Qilian Shan (north-eastern Tibet) by combining structural investigations, satellite imagery, topographic profiling, and ¹⁰Be exposure dating. We surveyed two terrace levels, and from each, we took 6–7 samples in profiles dug to depths of 2 m. These constrain inheritance and determine the precise ages of abandonment of the terraces: 29.9 ± 7.8 ka for the upper terrace and 16.3 ± 4.4 ka for the lower one. Topographic profiles with a determination of burial of the footwall by

sediment yield offsets of the surfaces of 96.4 ± 4.4 and 40.1 ± 2.8 m. The average vertical rate is 2.8 ± 1.3 mm a⁻¹ with a horizontal slip rate of ~ 2.5 mm a⁻¹. This rate is higher than those determined farther north on similar structures, but is consistent with the GPS velocity field, and accounts for roughly half of the geodetic shortening across the Qilian Shan.

Terra Nova, 22, 180–187, 2010

Introduction and tectonic setting

The Qilian Shan, with peak elevations > 5500 m, seems to have been built largely during the Late Miocene (e.g. Métivier *et al.*, 1998; Tapponnier *et al.*, 2001; Wang and Burchfiel, 2004; Zheng *et al.*, 2010) and continues to be seismically active (e.g. Tapponnier *et al.*, 1990), having produced very large earthquakes, e.g. $M = 8.5$, 1920, Haiyuan, and $M = 8.0$, 1927, Gulang earthquakes (Deng *et al.*, 1984; Gaudemer *et al.*, 1995; Zheng *et al.*, 2005). Associated deformation is partitioned into thrust faulting on planes dipping south–south-west and north–north-east and large sinistral strike–slip faulting on planes oriented WSW–ENE to WNW–ESE (e.g. Haiyuan–Qilianshan fault), as well as second-order dextral faults oriented NNW–SSW (Tapponnier and Molnar, 1977; Burchfiel *et al.*, 1991; Gaudemer *et al.*, 1995; Hetzel *et al.*, 2004b; Yuan *et al.*, submitted). The thickened crust of the Qilian Shan is due to reverse faulting in a region that seems to have grown east–north-eastward as the Altyn Tagh fault extended eastward (Burchfiel *et al.*, 1989; Tapponnier *et al.*, 1990; Métivier *et al.*, 1998). In this view, the Altyn Tagh fault crudely behaves as an intracontinental transform fault (e.g. Davis and Burchfiel,

1973), and the entire Qilian Shan as a continental-scale stepover (Fig. 1B). Our study area, an NW–SE elongated ‘valley’ between the Qilian Shan *s.s.* and the more external Long Shou Shan (Fig. 1B,C), is located on the main frontal thrust, north of the Haiyuan–Qilianshan and Gulang faults, and at the south-easternmost end of the Hexi Corridor. The studied thrust is the westernmost (west Shiyang) of the three right-stepping en-échelon E–W thrust faults noted by Gaudemer *et al.* (1995) that link the front of the Qilian Shan to the innermost Gulang and Haiyuan–Qilianshan faults (see fig. 106b in Gaudemer *et al.*, 1995). This indicates that sinistral shearing of the area is associated with the shortening that brings the pre-Devonian basement and its Mesozoic cover onto the Quaternary sediment of the footwall.

The aim of this study was to determine the slip rate of an E–W frontal thrust of the Qilian Shan south-east of the Hexi Corridor over a millennial time-scale by cosmogenic exposure age dating of terraces offset by the reverse fault.

Tectonic geomorphology

Fieldwork and aerial photo analyses

The studied area lies near the foot of the Qilian Shan, in the Hexi corridor, ~ 20 km to the NW of the city of Wuwei (Gansu Province), on the large alluvial fan of the Xiyang River (Fig. 2), i.e. where the river flows out of the belt onto the Tengger Desert.

This site lies a couple of kilometres west of the main river, the drainage area of which is ~ 1600 km². Upstream of our study area, Pan *et al.* (2006) dated three (of six) terraces, with ages ranging from *c.* 70 ka to *c.* 800 ka, as well as a higher erosion surface of *c.* 1300 ka, indicating a mean incision rate of ~ 0.1 mm a⁻¹. This area was chosen because of the well-preserved fault scarp, its easy access, and the occurrence of two clear, gently dipping, roughly planar surfaces ~ 20 and ~ 70 m above the surface of the footwall north of the scarp. These surfaces are lower than the ones dated by Pan *et al.* (2006) and have been ‘fossilized’ when the river cut into the fan and formed terraces. Quartz-rich pebbles and cobbles cover both surfaces that have undergone late incision of their edges by small ephemeral streams. Both surfaces, however, are well preserved, and the sharp transition between the top ‘flat’ surfaces and the eroding edges indicates that they have not undergone significant erosion by diffusive transport since their fossilization (Fig. 3).

The central part of the upper surface (S1, Fig. 3A,B) is approximately planar and preserved over an area of more than a half square kilometre. The lower surface (S2, Fig. 3C–E) is less affected by lateral erosion, but locally modified by farming. The fault scarp is visible on aerial photographs and satellite imagery (CORONA), as well as on the SRTM DEM (3'' resolution) and ASTER GDEM (1'' resolution). It is sharp and clear in the field, with a height of ~ 20 m (Fig. 3E).

Correspondence: Jean-Daniel Champagnac, Geological Institute - Earth Surface Dynamics, Sonneggstrasse 5, NO E 45, CH-8092 Zürich, Switzerland. e-mail: champagnac@gmail.com

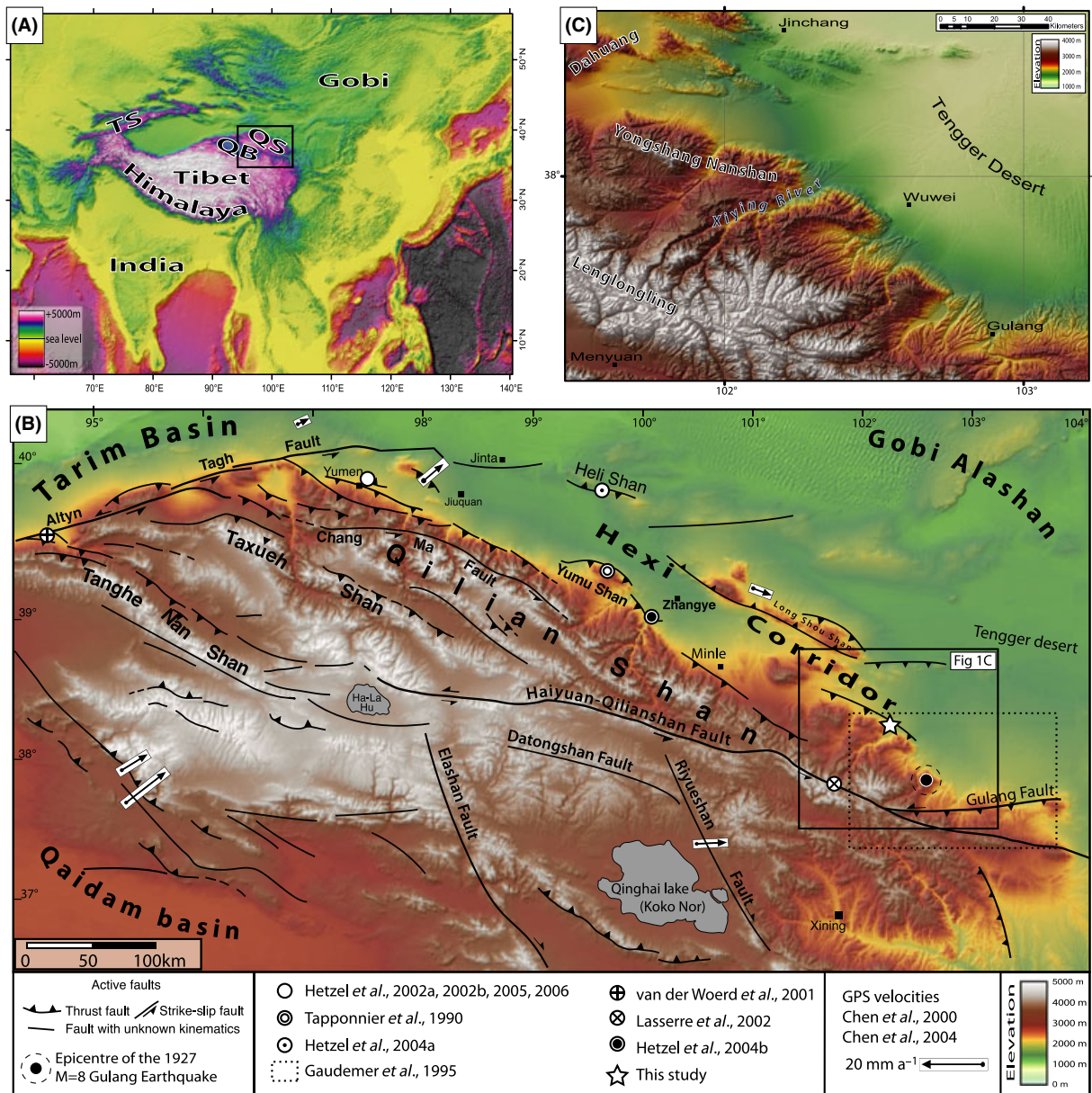


Fig. 1 Location of the study. (A) ETOPO2 DEM of Asia, with location and name of main ranges (TS, Tien Shan). The Cenozoic collision between India and Eurasia that occurred at *c.* 55–45 Ma has deformed a large intracontinental zone and created mountain ranges with high elevations over a broad area. The Qilian Shan (QS) is one of these mountain ranges and marks the north-eastern edge of the Tibetan Plateau, and is located north of the Qaidam Basin (QB). Black square locates (B). (B) GTOPO DEM of the south-eastern part of the Qilian Shan and location of main faults (after Gaudemer *et al.*, 1995; Meyer *et al.*, 1998; Hetzel *et al.*, 2004b). GPS velocities (Chen *et al.*, 2000, 2004), as well as location of previous neotectonic studies (Tapponnier *et al.*, 1990; Gaudemer *et al.*, 1995; van der Woerd *et al.*, 2001; Hetzel *et al.*, 2002a; Hetzel *et al.*, 2002b; Lasserre *et al.*, 2002; Hetzel *et al.*, 2004a; Hetzel *et al.*, 2004b; Hetzel and Hampel, 2005; Hetzel *et al.*, 2006), are also indicated. Black square locates (C). (C) SRTM DEM of the junction between the south-eastern end of the Hexi Corridor and the Qilian Shan frontal thrust. We did not add tectonic indications on the DEM to show the mountain front topography better. Note that the junction of the Lenglongling segment of the Haiyuan-Qilianshan fault and the Gulang fault (south of the city of Gulang) is clearly visible. Note also the fragmented nature of the frontal thrust, with a succession of NW–SE and E–W structures. This is due to the partition of the deformation between frontal shortening and the regional sinistral shearing.

The fault trace is oriented E–W, oblique to the general trend of the Qilian Shan and reaches the mountain front ~10 km farther west. Its E–W

orientation is similar to the fault scarp studied 150 km to the NW by Hetzel *et al.* (2004b) and to the Gulang fault (Gaudemer *et al.*, 1995).

Offset determination

To determine the offset, we carried out a topographic survey of the alluvial

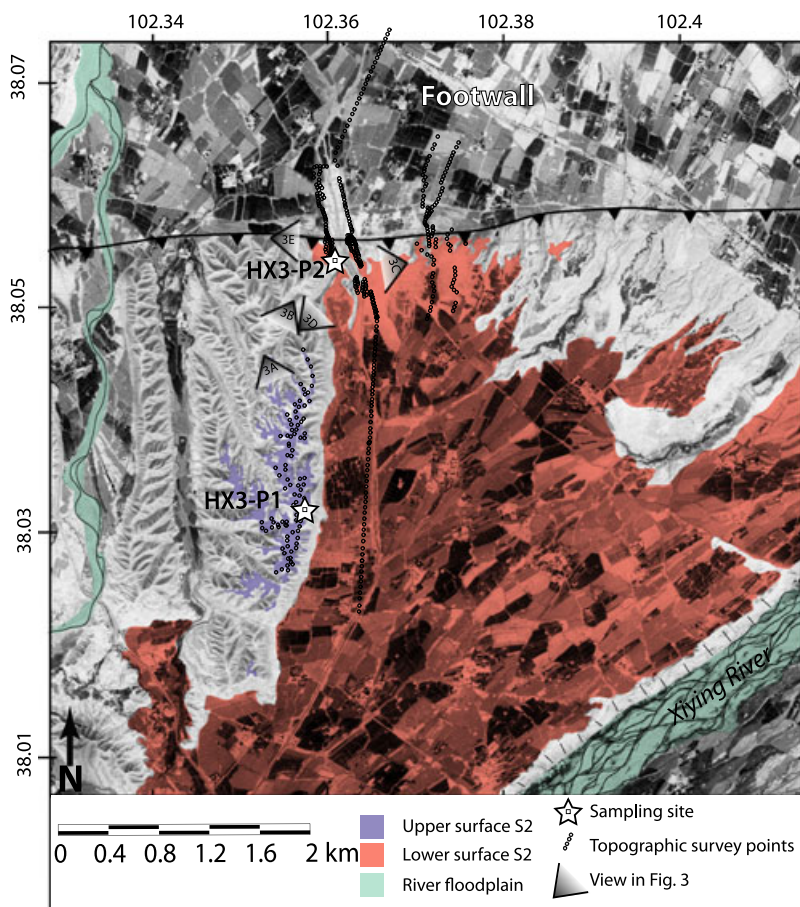


Fig. 2 Geomorphic map of the studied area. CORONA images (KH-4B-1101) provide high-resolution (1.8 m) background, coupled with fieldwork for geomorphological mapping of the studied area. Note that the topographic survey (small dots) ended on the footwall at its northern extent, because farther north, modification of the surface by humans made it unrepresentative of the natural topography. The dated surfaces are shown (upper surface S1, violet, and lower surface S2, pink), as well as active stream floodplains, sample locations and orientation of pictures in Fig. 3.

surfaces with a total station. We made one 4-km-long, and three 1-km-long topographic profiles on the lower surface S2 across the fault and on the footwall, as well as a mapping of a swath on the upper surface S1 (Fig. 2). The actual offsets of the surfaces were calculated by projecting elevations onto a profile perpendicular to the fault. We assigned the origin of the profile ($x = 0$) to foot of the fault scarp and we fitted straight lines to the elevation profiles on the two surfaces (S1 and S2) on the hangingwall, south of the fault scarp. Local variations as a result of erosion and folding, as well as erratic points, were omitted from the best fit calculation (Fig. 4).

The equation for the best fit line for the surface S2, south of the fault scarp, is height (m) = $-0.0161 \pm$

$0.0002x + 1737.3 \pm 0.2$ (m) with a $R^2 = 0.9662$. We assumed that the misfits to this line reflect folding caused by a slip on a surface that is not planar. We then fitted heights on the upper surface S1, assuming the same slope. The mild deformation of this surface makes it difficult to determine the precise slope. Moreover, we assumed that the depositional slope of the surface has not changed with time. For S1, the calculated best fit is height (m) = $-0.0161x + 1793.6 \pm 0.1$ (m), with a $R^2 = 0.9162$. This slope is close to the best fit value calculated with ‘slope’ as free parameter: height (m) = $0.0179 \pm 0.0005x + 1790.1 \pm 1.1$ (m), with a $R^2 = 0.9255$. This latter value of the slope provides an estimate of the uncertainty of the height intercept at the fault. The

difference between the two slopes is $0.0179 \pm 0.0005 - 0.0161 \pm 0.0002 = 0.0018 \pm 0.0005$. An evaluation of the uncertainty in height intercept at the fault is given by the slope uncertainty times the distance between from centre of the profile (2630 – 1180 m = 1450 m), combined with the numerical uncertainty of the linear best fit. The final uncertainty of the height of S1 at the fault ($x = 0$) is ± 3.4 m.

The displacement caused by slip on the fault, however, requires consideration of possible burial of the footwall by sediment. To determine a minimal value of the burial of the footwall (b) after the fault offset, we assumed that the thickness of sediment decreases exponentially from the fault. Thus, we fitted heights to a sum of a linear term and an exponential term that decreases with distance from the fault. For the linear part, we assumed the slope we estimated for S2 to be 0.0161. Thus, we fitted $h(x) = h_0(x = 0) + 0.0161x + b \exp(kx)$. Here, b gives the burial of the footwall by sediment at the fault trace, and h_0 gives the elevation of the footwall surface at the fault.

For the eastern, central and western profiles, we obtained $b = 20.7 \pm 1.2$, 19.0 ± 0.3 and 27.0 ± 6.3 m respectively with a mean of 22.2 ± 2.6 m. More importantly, the elevations of the footwall surface at the fault are $h_0 = 1694.6 \pm 6.6$, 1701.7 ± 0.4 and 1695.3 ± 1.5 m, with an average of 1697.2 ± 2.8 m. The corresponding vertical component of offset of surface S1 is therefore $1793.6 \pm 3.4 - 1697.2 \pm 2.8 = 96.4 \pm 4.4$ m. Similarly, the vertical component of displacement of the surface S2 is $1737.3 \pm 0.2 - 1697.2 \pm 2.8 = 40.1 \pm 2.8$ m.

Surface exposure ages

To constrain the ages of abandonment of both terrace surfaces, we used the amalgamation method of Anderson *et al.* (1996). For each sample, we took a large number ($n > 50$) of cm-size, quartz-rich pebbles in vertical profiles from two pits. Pit P1 was dug in the upper surface (S1) to a depth of 2 m, away from the edge and gullies (Fig. 5 A). We dug a trench into the lower surface (S2), a few tens of metres away from the fault scarp, at the side of a fresh road excavation (Fig. 5B).

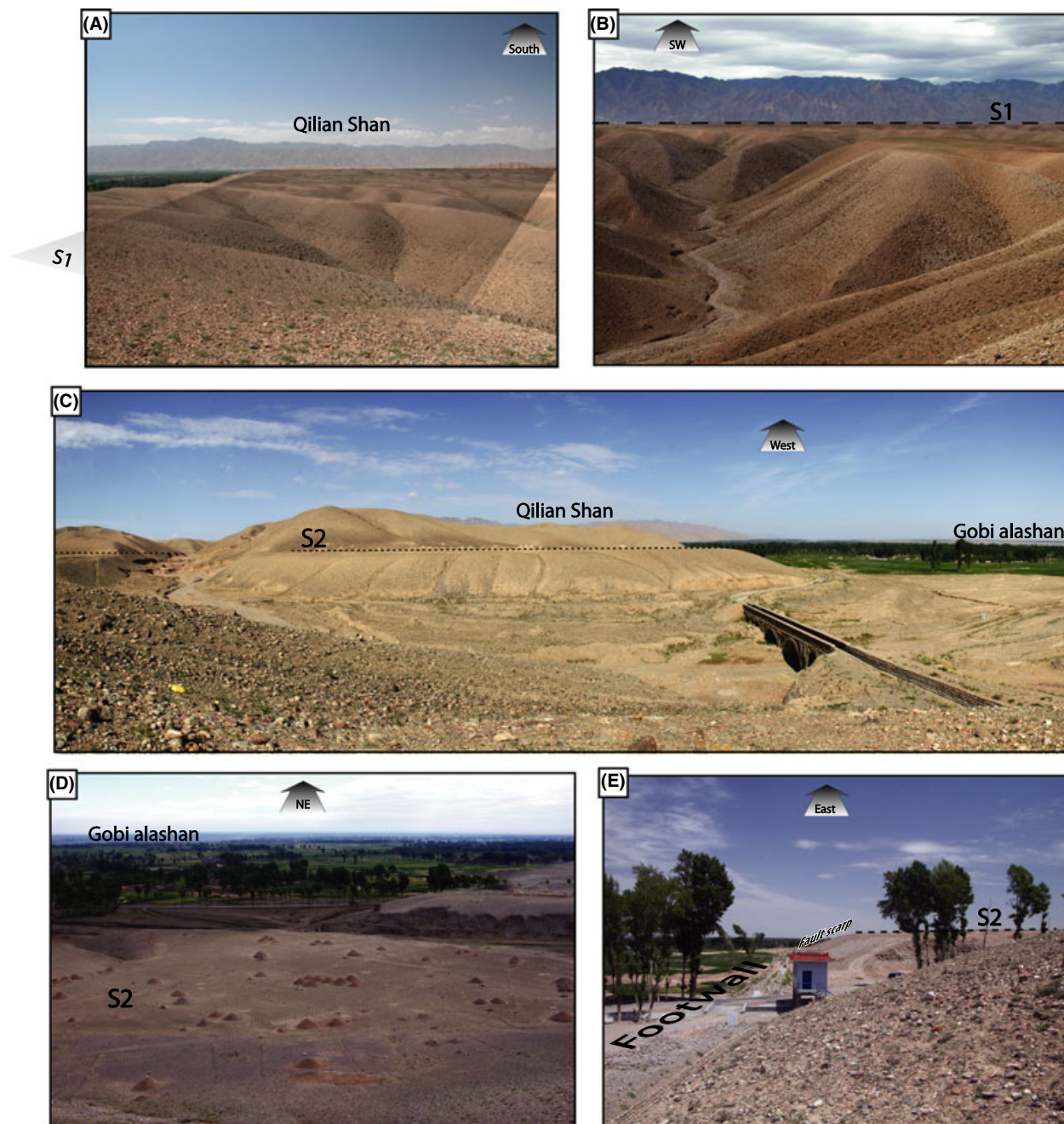


Fig. 3 Field photographs of the studied surfaces. (A,B) Views of the upper surface S1 towards the SSW. Note the importance of flat remnant of the palaeosurface between the gullies, allowing a precise topographic survey. The Qilian Shan high peaks are in the background. (C) Side view of the lower surface S2, the fault scarp on its right edge, and the footwall farther to the right. The bridge is an aqueduct, crossing the Xiying River. (D) View towards the north-east of the lower surface S2, and the fault scarp, from the upper surface. The little cone-like structures are graves of 1–2 m height. (E) Along-strike view of the fault scarp, towards the east. Note the sharp transitions between the surface S2 and the scarp, and between the scarp and the footwall.

We calculated ages (Table 1) using the MS excel calculator Cosmocalc (Vermeesch, 2007). We fitted ^{10}Be concentration vs. depth to function consisting of a constant plus an exponential decay with depth (e.g. Anderson *et al.*, 1996; Farber *et al.*, 2008).

The constant in this expression provides an estimate of the average concentration ^{10}Be in samples prior to deposition, or ‘inheritance’, which, for our samples, is very small (equivalent to a couple of hundred years at most). The pre-factor of the expo-

ponential term provides an estimate of the cosmic rays accumulated since the abandonment of the surface (Fig. 5C,D). This value is not necessarily equal to the concentration of the surface sample, but takes into account concentrations in all the

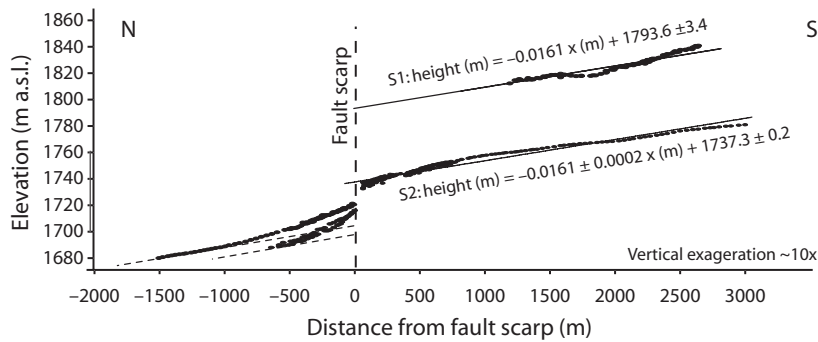


Fig. 4 Topographic survey points projected onto an N–S vertical plane. A linear interpolation of the relevant survey points along S2 yields a best fit line given by height (m) = $-(0.0161 \pm 0.0002)x$ (m) + 1737.3 ± 5 with $R^2 = 0.97$. We assume, however, an error of 5 m to allow for deviations from a planar surface of the terrace. Clearly, some folding of that surface is possible, if a fit that included folding of the surface in the 1000 m near the fault would project to a higher elevation at the scarp, and we consider this unlikely. We imagine, however, that deviations from a planar surface merely reflect remnants of the drainage pattern on the surface when it was abandoned to form the terrace. We presume that the surfaces S1 and S2 formed with the same slope, since for where we could measure it, S1 stands at relatively constant elevation, 55–60 m above S2. Assuming the same slope, a least-squares fit to S1 yields a difference in height of relatively constant 57 ± 7 m. The surface north of the scarp is clearly not planar, but surely on the distance scale that we consider, the northward projections of S1 or S2 would be planar. The deviation from a planar surface is a manifestation of sediment accumulation caused by erosion of the scarp and by transport by streams that have dissected the terraces. The thickness of the sediment obviously decreases northward, but also varies along the scarp from east to west. We assumed that the thickness of that sediment varies exponentially from the scarp and fitted a curve of the form of a linear slope (of 0.0161) plus an exponential curve to the height: $h(x) = h_0 + 0.0161x + b \exp(kx)$. We note that we have no theory to justify an exponential fit, but the good fits that we obtain suggest that this is a reasonable approximation to the shape of the surface. Thus, here b gives the burial of the footwall by the sediment at the fault trace, and h_0 gives the elevation of the footwall surface at the fault. For the eastern, central and western profiles, we obtained $b = 21 \pm 1, 19 \pm 1$ and 27 ± 6 m, respectively, with a mean of 22 ± 3 m. More importantly, the elevations of the footwall surface at the fault are $h_0 = 1695 \pm 7, 1702 \pm 1$ and 1695 ± 2 m, with an average of 1697 ± 3 m. The corresponding vertical component of offset of surface S1 is therefore $1794 \pm 5 - 1697 \pm 3 = 97 \pm 6$ m. Similarly, the vertical component of displacement of the surface S2 is $1737 \pm 5 - 1697 \pm 3 = 40 \pm 6$ m.

samples to determine the age of exposure.

Best fit equations of ^{10}Be concentration per gram of SiO_2 related to depth (Table 1) are:

$$[^{10}\text{Be}(\# \text{ g}^{-1})] = [39\,446 \pm 63\,749] + [(636\,710 \pm 59\,376) \times e^{-0.0125z(\text{m})}]$$

and

$$[^{10}\text{Be}(\# \text{ g}^{-1})] = [0 \pm 38\,582] + [(326\,000 \pm 37\,871) \times e^{-0.0125z(\text{m})}]$$

for S1 and S2 respectively.

The factor in the exponential term (0.0125 m^{-1}) was chosen to maximize the best fit for both profiles (Fig. 6). This corresponds to a sediment density of 1.8 mg m^{-3} for an apparent attenuation length of ^{10}Be production of 145 g cm^{-2} (Brown *et al.*, 1992), a density of 2.0 mg m^{-3} for an attenuation length of 160 g cm^{-2} (Nishiizumi *et al.*, 1994), or a slightly higher density of 2.2 mg m^{-3} for an attenuation length of 177 g cm^{-2} (Farber *et al.*, 2008). This is consistent with sediment densities used by previous studies (e.g. $2.0 \pm 0.1 \text{ mg m}^{-3}$, Ritz

et al. 2003; $2.0 \pm 0.3 \text{ mg m}^{-3}$, Brocard *et al.* 2003).

To estimate ages from the concentrations at the surface, we used a low-elevation, high-latitude production rate of $5.11 \text{ at. a}^{-1} \text{ g}^{-1} \text{ SiO}_2$ (Vermeesch, 2007). This rate was then adjusted for elevation and latitude of the site where we worked, using Stone’s (2000) formulation. The actual production rate for our sites is $19.98 \pm 2 \text{ at. a}^{-1} \text{ g}^{-1}$. This yields ages corresponding to the inheritance of 2 ± 3.8 and $0 \pm 2 \text{ ka}$ for S1 and S2 respectively and apparent exposure ages of $31.9 \pm 6.8 \text{ ka}$ for S1 and $16.3 \pm 3.9 \text{ ka}$ for S2. Therefore, ages corrected for inheritance are 29.9 ± 7.8 and $16.3 \pm 4.4 \text{ ka}$ for S1 and S2 respectively.

Late Quaternary slip rate

Consider the simple image in Fig. 7, in which let us consider ΔH_1 to be the height of the surface S1 above palaeo-surface of the footwall at the fault trace, and ΔH_2 be the same as for S2. Let b = thickness of the sediment deposited on the footwall since fault-

ing occurred. We use t_1 and t_2 for the ages S1 and S2 respectively. With these, the vertical component of slip on the fault v' is given by:

$$v'_1 = \Delta H_1 / t_1$$

and

$$v'_2 = \Delta H_2 / t_2$$

with $\Delta H_1 = 96.4 \pm 4.4 \text{ m}$, $\Delta H_2 = 40.1 \pm 2.8 \text{ m}$, $t_1 = 29.9 \pm 7.8 \text{ ka}$, $t_2 = 16.3 \pm 4.4 \text{ ka}$, $v'_1 = 3.2 \pm 1.0 \text{ mm a}^{-1}$ and $v'_2 = 2.5 \pm 0.8 \text{ mm a}^{-1}$. These two values agree with each other, within errors. Their average is $2.8 \pm 1.3 \text{ mm a}^{-1}$.

The dip of the frontal thrust of the Qilian Shan and the studied thrust fault remains unknown. Meyer *et al.* (1998) documented thrust faults from balanced cross-sections with a dip of 40° – 65° . Hetzel *et al.* (2004b) argued that the Zhangye thrust, similar to the thrust fault in our study, is a probable reactivation of Mesozoic normal fault, with a probable dip of $50^\circ \pm 10^\circ$. Gaudemer *et al.* (1995) assumed a dip of $45^\circ \pm 15^\circ$ for the Xiyang ramp.

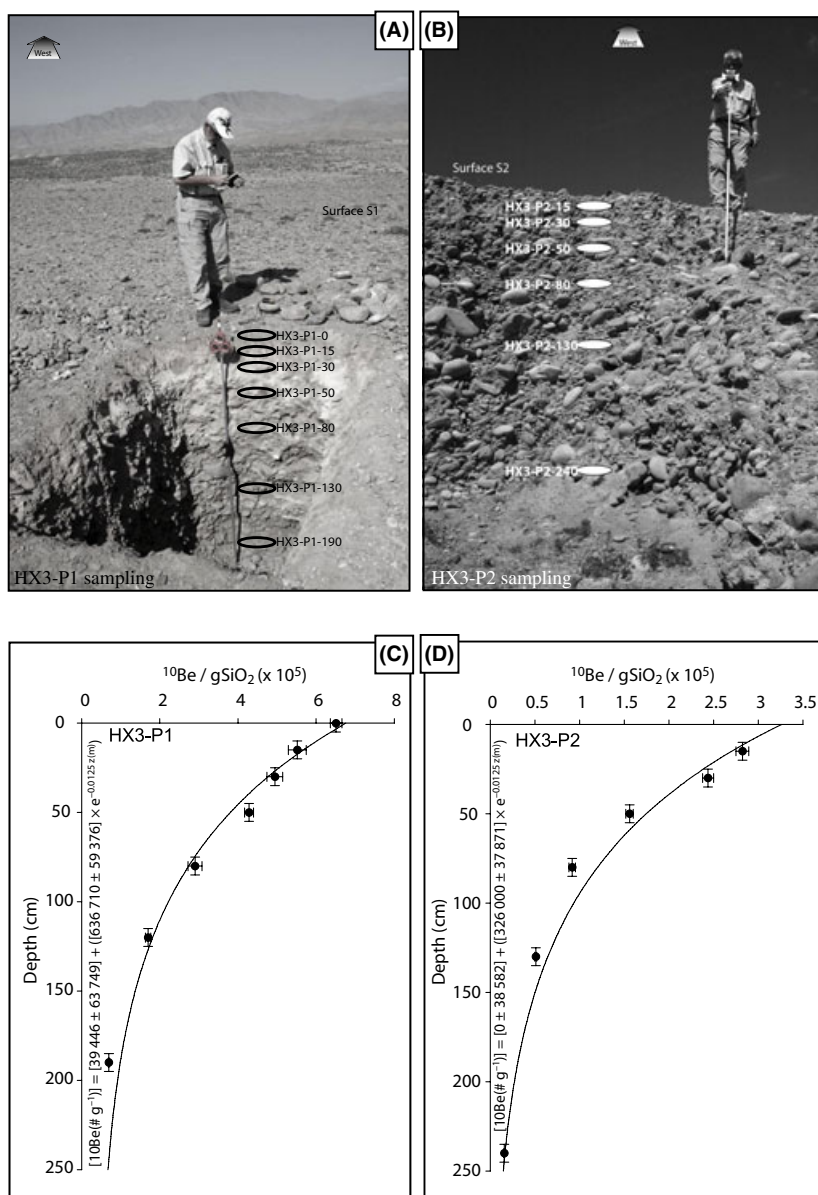


Fig. 5 (A) Photograph of sampling site on S1 showing the setting of the pit P1. PM (1.83 m) gives the scale. Seven samples were taken at the surface and at depths below 15, 30, 50, 80, 120 and 190 cm. (B) Pictures of sampling site on S2 showing the setting of the pit P2. PM again gives the scale. Six samples were taken at depths of 15, 30, 50, 80, 130 and 240 cm. (C,D) Plots of concentrations of ^{10}Be vs. depth for sample sets HX3-P1 and HX3-P2 (reported errors are 1 sigma). Exponential best fits, for a density of sediment = 2.0 (spallation attenuation length of 160 cm), as well as positive (or null) asymptotic values, yield ^{10}Be at surface. This value, as well as the inheritance (^{10}Be concentration at depth), is used to determine exposure ages of the surfaces. As noted by Farber *et al.* (2008), neutron-induced spallation is the predominant production mechanism in the upper ~ 3 m of a depth profile. Quartz extraction was performed in the University of Colorado at Boulder facility, using standard chemical cleaning and etching, as well as heavy liquid separation. Pure quartz samples (tested at the University of Colorado for low Al content) were sent to Purdue Rare Isotope Measurement Laboratory (PRIME lab, Purdue University, USA) for further chemical treatment and accelerator mass spectrometry (AMS) measurement. Results (Table 1) were provided by PRIME as $^9\text{Be}/^{10}\text{Be}$, using the ICN standard (Nishiizumi *et al.*, 2007).

This dip yields a horizontal slip rate across the fault similar to the vertical movement of $2.8 \pm 1.3 \text{ mm a}^{-1}$, but uncertainties on the fault orientation at depth prevent a precise calculation.

Conclusions

The vertical and horizontal rates determined in this study contrast with lower rates determined farther north by Hetzel *et al.* (2004b) on a similar thrust fault. The Zhangye thrust (Hetzel *et al.*, 2004b) is located in front of the north-verging ‘back’ thrusts of the Long Shou Shan and therefore lies in a more internal part of the Qilian Shan than the fault we studied. This is consistent with the Qilian Shan front currently propagating into the Alashan plateau. Our results are consistent with GPS constraints, which show NNE–SSW shortening across the Qilian Shan at a rate of $5.5 \pm 1.8 \text{ mm a}^{-1}$ (Zhang *et al.*, 2004). Slip on the thrust fault we studied for millennial time-scale accounts for a significant fraction ($\sim 50\%$), but almost surely not the entire geodetic shortening across the entire Qilian Shan. This rate, which is comparable with that of some of reverse faults in the Tien Shan (e.g. Burchfiel *et al.*, 1999; Thompson *et al.*, 2002), supports the image that Qilian Shan and the adjacent Hexi Corridor deform by slip on more than one major fault. Although the 1927 Gulang earthquake rupture seems to have stopped south-east of the reverse fault we studied (Repetti, 1928; Gaudemer *et al.*, 1995), clearly, the shortening rate of $\sim 2.5 \text{ mm a}^{-1}$ suggests that such an earthquake might be rare on human time-scales, but should recur at intervals of *c.* 1000 years. We also observed that vertical and horizontal components of the slip are notably higher than the average rates of 0.5 and 0.9 mm a^{-1} that Zheng *et al.* (2010) estimated for the past 9 Ma, from the region to the north-west. We do not associate the higher late Quaternary rates with an acceleration in the convergence rate, but rather with a northward progression of the locus of active deformation. We thank two anonymous reviewers and the editor (Carlo Doglioni) for constructive comments that improved a previous version of the manuscript.

Table 1 Location, depth and concentration in ¹⁰Be of samples used in this study.

Coordinates			Sample		Weight		¹⁰ Be/total (E-15)		¹⁰ Be concentration				
X	Y	alt.	Name	Depth (cm)	Weight SiO ₂	Weight ⁹ Be (mg)	Value	Error	¹⁰ Be atoms	¹⁰ Be at. g ⁻¹ SiO ₂	Error		
102.35455	38.03225	1841	HX3-P1-0	0–5	59.4259987	0.296525	21 687	493	38 684 171	650 964	14 811		
			HX3-P1-15	10–20	21.1809998	0.298265	6528	268	11 683 303	551 594	22 693		
			HX3-P1-30	25–35	13.5587997	0.29899	3745	152	6 700 861	494 208	20 185		
			HX3-P1-50	43–57	32.5712013	0.297975	7798	210	13 950 839	428 318	11 580		
			HX3-P1-80	70–90	28.2807999	0.2987	4581	280	8 198 135	289 883	17 828		
			HX3-P1-120	110–130	47.8017998	0.29812	4550	179	8 126 562	170 005	6726		
			HX3-P1-190	180–200	35.5343018	0.2982	1402	40	2 475 025	69 652	2016		
102.36073	38.05455	1742	HX3-P2-15	10–20	40.1637993	0.296815	6362	162	11 323 734	282 090	7210		
			HX3-P2-30	25–35	43.1599985	0.29986	5845	147	10 512 449	243 569	6146		
			HX3-P2-50	45–55	21.7964001	0.297395	1919	51	3 394 908	155 755	4164		
			HX3-P2-80	73–87	35.8415985	0.298265	1847	73	3 275 516	91 389	3672		
			HX3-P2-130	120–140	41.4513016	0.29667	1202	27	2 105 678	50 799	1182		
			HX3-P2-240	230–250	43.2938004	0.29667	394	16	662 505	15 303	656		
			Cblk1440-0	–	–	–	–	–	23.37	3.8	–	–	–

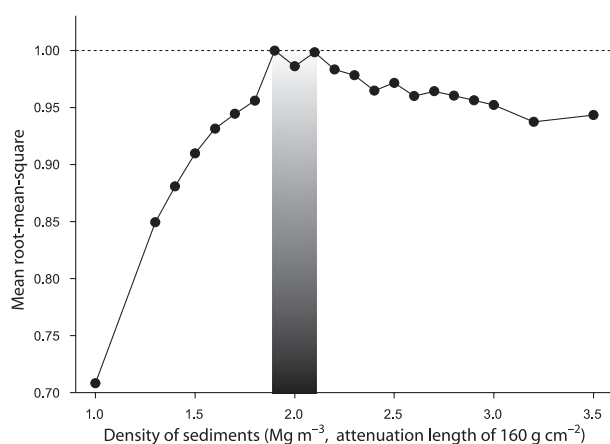


Fig. 6 Impact of the sediment density on the exponential best fit of the ¹⁰Be concentration with depth. Best values are given by a factor in the exponential term of 0.0125, corresponding to a density of 2.0 mg m⁻³, for a fast neutron attenuation length of 160 g cm⁻². This value is similar to actual sediment density.

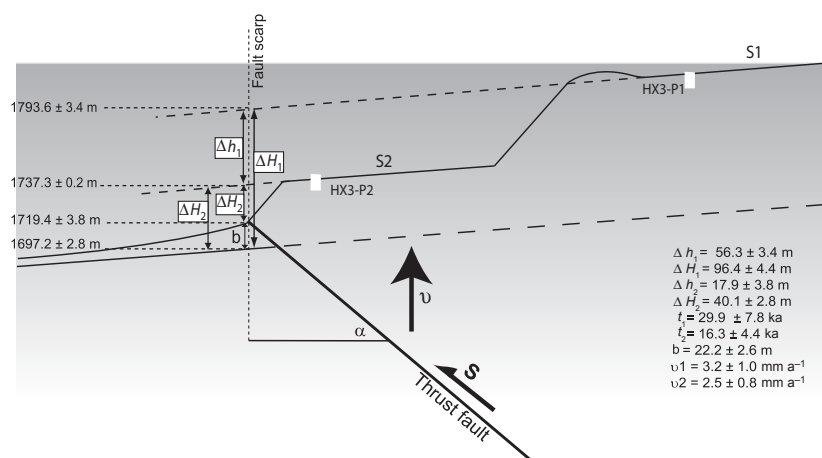


Fig. 7 Cartoon sketch of the fault zone and the dated surfaces, with the variables used in the calculations, as well as values and uncertainties of these variables. The minimum burial *b* is determined by the fit of a sum of a linear slope and an exponential that decreases from the fault (see Offset determination), and $\Delta H_1 = b + \Delta h_1$, and $\Delta H_2 = b + \Delta h_2$.

Acknowledgements

This work was supported by the National Science Foundation of the USA under grant EAR 0507330 and by the Swiss National Science Foundation under the grants # PBNE2-106764, # PA002-117441 and PZ00P2_126408/1. We thank R. S. Anderson and D. Ward for help with ¹⁰Be sample preparation. All the cosmogenic radionuclide calculations were performed using Cosmocalc (Vermeesch, 2007). We thank two anonymous reviewers and the editor (Carlo Doglioni) for constructive comments that improved a previous version of the manuscript. We also thank Kevin Norton for this help in figure preparation.

References

Anderson, R.S., Repka, J.L. and Dick, G.S., 1996. Dating depositional surfaces using in situ produced cosmogenic radionuclides. *Geology*, **24**, 47–51.

Brocard, G.Y., van der Beek, P.A., Bourlès, D.L., Siame, L.L. and Mugnier, J.L., 2003. Long-term fluvial incision rates and postglacial river relaxation time in the French Western Alps from ¹⁰Be dating of alluvial terraces with assessment of inheritance, soil development and wind ablation effects. *Earth and Planetary Science Letters*, **209**, 197–214.

Brown, E.T., Brook, E.J., Raisbeck, G.M., Yiou, F. and Kurtz, M.D., 1992. Effective attenuation lengths of cosmic-rays producing Be-10 and Al-26 in quartz: implications for exposure age dating. *Geophys. Res. Lett.*, **19**, 369–372.

Burchfiel, B.C., Deng, Q.-D., Molnar, P., Royden, L., Wang, Y.-P., Zhang, P.-Z. and Zhang, W.-Q., 1989. Intracrustal detachment within zones of continental deformation. *Geology*, **17**, 448–452.

Burchfiel, B.C., Zhang, P., Wang, Y., Zhang, W., Song, F., Deng, Q., Molnar, P. and Royden, L.H., 1991. *Geology of*

- the Haiyuan fault zone, Ningxia-Hui Autonomous region, China, and its relation to the evolution of the north-eastern margin of the Tibetan Plateau. *Tectonics*, **10**, 1091–1110.
- Burchfiel, B.C., Brown, E.T., Qidong, D., Xianyue, F., Jun, L., Molnar, P., Jianbang, S., Zhangming, W. and Huichuan, Y., 1999. Crustal shortening on the margins of the Tien Shan, Xinjiang, China. *Int. Geol. Rev.*, **41**, 665–700. doi:10.1080/00206819909465164.
- Chen, Q., Freymueller, J.T., Wang, Q., Yang, Z., Xu, C. and Liu, J., 2004. A deforming block model for the present-day tectonics of Tibet. *Journal of Geophysical Research B: Solid Earth*, **109**, B01403 01401–01416.
- Chen, Z., Burchfiel, B.C., Liu, Y., King, W., Royden, L.H., Tang, W., Wang, E., Zhao, J. and Zhang, X., 2000. Global Positioning System measurements from eastern Tibet and their implications for India/Eurasia intercontinental deformation. *Journal of Geophysical Research B: Solid Earth*, **105**, 16215–16227.
- Davis, G.A. and Burchfiel, B.C., 1973. Garlock fault; An intracontinental transform structure, Southern California. *Geol. Soc. Am. Bull.*, **84**, 1407–1422.
- Deng, Q., Song, F., Zhu, S., Li, M., Wang, T., Zhang, W., Burchfiel, B.C., Molnar, P. and Zhang, P., 1984. Active faulting and tectonics of the Ningxia-Hui autonomous region, China. *J. Geophys. Res. B*, **89**, 4427–4445.
- Farber, D.L., Mériaux, A.-S. and Finkel, R.C., 2008. Attenuation length for fast nucleon production of ^{10}Be derived from near-surface production profiles. *Earth Planet. Sci. Lett.*, **274**, 295–300.
- Gaudemer, Y., Tapponnier, P., Meyer, B., Peltzer, G., Shunmin, G., Zhitai, C., Huang, D. and Cifuentes, I., 1995. Partitioning of crustal slip between linked, active faults in the eastern Qilian Shan, and evidence for a major seismic gap, the “Tianzhu gap”, on the western Haiyuan Fault, Gansu (China). *Geophys. J. Int.*, **120**, 599–645.
- Hetzl, R., Niedermann, S., Ivy-Ochs, S., Kubik, P.W., Tao, M. and Gao, B., 2002a. ^{21}Ne versus ^{10}Be and ^{26}Al exposure ages of fluvial terraces: the influence of crustal Ne in quartz. *Earth Planet. Sci. Lett.*, **201**, 575–591.
- Hetzl, R., Niedermann, S., Tao, M., Kubik, P.W., Ivy-Ochs, S., Gao, B. and Strecker, M.R., 2002b. Low slip rates and long-term preservation of geomorphic features in Central Asia. *Nature*, **417**, 428–432.
- Hetzl, R., Tao, M., Niedermann, S., Strecker, M.R., Ivy-Ochs, S., Kubik, P.W. and Gao, B., 2004a. Implications of the fault scaling law for the growth of topography: mountain ranges in the broken foreland of north-east Tibet. *Terra Nova*, **16**, 157–162.
- Hetzl, R., Tao, M., Stokes, S., Niedermann, S., Ivy-Ochs, S., Gao, B., Strecker, M.R. and Kubik, P.W., 2004b. Late Pleistocene/Holocene slip rate of the Zhangye thrust (Qilian Shan, China) and implications for the active growth of the northeastern Tibetan Plateau. *Tectonics*, **23**, 1–17.
- Hetzl, R., Niedermann, S., Tao, M., Kubik, P.W. and Strecker, M.R., 2006. Climatic versus tectonic control on river incision at the margin of NE Tibet: 10Be exposure dating of river terraces at the mountain front of the Qilian Shan. *J. Geophys. Res. F. Earth Surf.*, **111**, F03012. doi:10.1029/2005JF000352.
- Métivier, F., Gaudemer, Y., Tapponnier, P. and Meyer, B., 1998. Northeastward growth of the Tibet plateau deduced from balanced reconstruction of the two areas: the Qaidam and Hexi corridor basins, China. *Tectonics*, **17**, 823–842.
- Meyer, B., Tapponnier, P., Bourjot, L., Métivier, F., Gaudemer, Y., Peltzer, G., Shunmin, G. and Zhitai, C., 1998. Crustal thickening in Gansu-Qinghai, lithospheric mantle subduction, and oblique, strike-slip controlled growth of the Tibet plateau. *Geophys. J. Int.*, **135**, 1–47.
- Nishiizumi, K., Finkel, R.C., Caffee, M.W., Southon, J.R., Kohl, C.P., Arnold, J.R., Olinger, C.T., Poths, J. and Klein, J., 1994. Cosmogenic production of ^{10}Be and ^{26}Al on the surface of the earth and underground. *Eighth International Conference on Geochronology, Cosmochronology and Isotope Geochemistry*. U.S. Geological Survey Circular 07, Berkeley, CA, 234 pp.
- Nishiizumi, K., Imamura, M., Caffee, M.W., Southon, J.R., Finkel, R.C. and McAninch, J., 2007. Absolute calibration of ^{10}Be AMS standards. *Nucl. Instrum. Meth. Phys. Res. B*, **258**, 403–413.
- Pan, B.-T., Gao, H.-S., Wu, G.-J., Li, J.J., Li, B.-Y. and Ye, Y.-G., 2006. Dating of erosion surface and terraces in the eastern Qilian Shan, northwest China. *Earth Surf. Proc. Land.*, **32**, 143–154.
- Repetti, W.C. 1928. The epicenter of the Kansu earthquake of May 23, 1927. *Bull. Seismol. Soc. Am.*, **18**, 1–14.
- Ritz, J.F., Bourlès, D., Brown, E.T., Carretier, S., Chéry, J., Enhtuvshin, B., Galsan, P., Finkel, R.C., Hanks, T.C., Kendrick, K.J., Philip, H., Raisbeck, G., Schlupp, A., Schwartz, D.P. and Yiou, F., 2003. Late Pleistocene to Holocene slip rates for the Gurvan Bulag thrust fault (Gobi-Altay, Mongolia) estimated with ^{10}Be dates. *Journal of Geophysical Research B: Solid Earth*, **108**, ETG 8-1–8-16.
- Stone, J.O., 2000. Air pressure and cosmogenic isotope production. *J. Geophys. Res. B. Solid Earth*, **105**, 23753–23759.
- Tapponnier, P. and Molnar, P., 1977. Active faulting and tectonics in China. *J. Geophys. Res. B*, **82**, 2905–2930.
- Tapponnier, P., Meyer, B., Avouac, J.P., Peltzer, G., Gaudemer, Y., Guo, S.-M., Xiang, H.-F., Yin, K., Chen, Z.-T., Cai, S.-H. and Dai, H.-G., 1990. Active thrusting and folding in the Qilian Shan, and decoupling between upper crust and mantle in northeastern Tibet. *Earth Planet. Sci. Lett.*, **97**, 382–403.
- Tapponnier, P., Xu, Z.-Q., Roger, F., Meyer, B., Arnaud, N., Wittlinger, G. and Yang, J.-S., 2001. Oblique stepwise rise and growth of the Tibet plateau. *Science*, **294**, 1671–1677.
- Thompson, S.C., Weldon, R.J., Rubin, C.M., Abdrakhmatov, K., Molnar, P. and Berger, G.W., 2002. Late Quaternary slip rates across the central Tien Shan, Kyrgyzstan, central Asia. *J. Geophys. Res. B. Solid Earth*, **107**, ETG 7-1 to 7–32. doi:10.1029/2001JB000596.
- Van Der Woerd, J., Xiwei, X., Haibing, L., Tapponnier, P., Meyer, B., Ryerson, F.J., Meriaux, A.-S. and Zhiqin, X., 2001. Rapid active thrusting along the northwestern range front of the Tanghe Nan Shan (western Gansu, China). *J. Geophys. Res. B. Solid Earth*, **106**, 30475–30504.
- Vermeesch, P., 2007. CosmoCalc: an Excel add-in for cosmogenic nuclide calculations. *Geochem. Geophys. Geosyst.*, **8**, Q08003. doi:10.1029/2006GC001530.
- Wang, E. and Burchfiel, B.C., 2004. Late Cenozoic right-lateral movement along the Wenquan fault and associated deformation: implications for the kinematic history of the Qaidam Basin, northeastern Tibetan Plateau. *Int. Geol. Rev.*, **46**, 861–879.
- Yuan, D.-Y., Champagnac, J.-D., Ge, W.-P., Molnar, P., Zhang, P.-Z., Zheng, W.-J. and Zhang, H.P., 2010. Late Quaternary right-lateral slip rates of active faults adjacent to lake Qinghai, northeastern margin of the Tibetan Plateau. *Geol. Soc. Am. Bull.* (in press).
- Zhang, P.-Z., Shen, Z., Wang, M., Gan, W., Burgmann, R., Molnar, P., Wang, Q., Niu, Z., Sun, J., Wu, J., Sun, H. and You, X., 2004. Continuous deformation of the Tibetan Plateau from global positioning system data. *Geology*, **32**, 809–812.
- Zheng, W.-J., Yuan, D.-Y., Zhang, D.-L., He, W.-G., Guo, H. and Liu, B.-Q., 2005. Rupture property of the 1927 Gulang M_s 8.0 Earthquake and numerical simulation of rupture mechanism. *Earthquake Res. China*, **19**, 409–419.
- Zheng, D.-W., Clark, M.K., Zhang, P.-Z., Zheng, W.-J. and Farley, K.A., 2010. Erosion, fault initiation and topographic growth of the North Qilian Shan (northern Tibetan Plateau). *Geosphere*, **28**, 715–718.

Received 13 January 2010; revised version accepted 15 January 2010